Cu^{3+}/Ni^{3+} Dual Active Sites for High-Voltage Driven Electrocatalytic Production of 2,5-Furanedicarboxylic acid

Baoming Yan [a], Hongliang Dai [a], Mengyang Yin [a], Chen Hao [a], Yutang Shen [a], Hongye Bai [a, *], Ying Liu [c, *], Guohai Xu [b, *], Weiqiang Fan [a, *]

[a] *School of Chemistry and Chemical Engineering, Jiangsu University, Zhenjiang, 212013, PR China.*

[b] *Key Laboratory of Jiangxi University for Functional Materials Chemistry, School of Chemistry and Chemical Engineering, Gannan Normal University, Ganzhou, 341000, PR China.*

[c] *Multi-scale Porous Materials Center, Institute of Advanced Interdisciplinary Studies & School of Chemistry and Chemical Engineering, Chongqing University, Chongqing 400044, PR China.*

* *Corresponding author. bhy198412@163.com, liuying11@cqu.edu.cn, xuguohai@gnnu.edu.cn fwq4993329@ujs.edu.cn*

1. Experimental section

1.1. Chemicals and Reagents.

Nickel foam (NF) and $Cu(NO_3)_2 \cdot 3H_2O$ (98%) were purchased from Macklin. HMF, FDCA, furan-2,5-dicarbaldehyde (DFF), 5-formyl-2-furancarboxylic acid (FFCA), and 5-hydroxymethyl-2-furancarboxylic acid (HMFCA) were purchased from Macklin.

1.2. Synthesis of Ni_3S_2.

NF was sliced into approximately 2 cm × 3 cm pieces and washed sequentially in 1 mol L^{-1} HCl solution, anhydrous ethanol, and deionized water for 30 min. NF was then vacuum dried at 60 °C overnight. Afterward, a piece of cleaned NF was immersed in 30 mL thiourea aqueous solution (1.5 mM). Then, it was transferred to an autoclave and maintained at 140 ℃ for 12 h. The prepared Ni_3S_2 were rinsed repeatedly with deionized water and dried at 60 °C overnight.

1.3. Synthesis of Cu-NF.

NF was sliced into approximately 1 cm × 2 cm pieces, Cu-NF was prepared by electrodeposition via a three-electrode system at -1.2 V vs Ag/AgCl (25 °C). The electrolyte solution was obtained by dissolving $Cu(NO_3)_2 \cdot 3H_2O$ (1.2 g) in deionized water (50 mL). The prepared Cu-NF samples were rinsed repeatedly with deionized water and dried at 60 °C overnight.

1.4. Synthesis of Cu-Ni_3S_2.

Ni_3S_2 sample was cut into 1 cm × 2 cm pieces. Cu-Ni_3S_2 was prepared by electrodeposition in a three-electrode system at -1.2 V vs Ag/AgCl (25 °C) with $Cu(NO_3)_2$ electrolyte. The prepared samples were repeatedly rinsed with deionized water to remove residual electrolyte from the surface and dried overnight at 60 °C.

1.5. Characterization.

Morphological characterization of the samples was studied using scanning

electron microscopy (SEM, Apreo S HiVac) and high-resolution transmission electron microscopy (HR-TEM, JEM-2100). Crystallographic phase analysis was performed by X-ray diffraction (XRD, SmartLab). Chemical composition and valence states were evaluated by X-ray photoelectron spectroscopy (XPS, ESCALAB QXi). Raman spectroscopy (Raman, DXR) was utilized to obtain information on the molecular structure and determine the chemical bonds.

1.6. Electrochemical Measurements.

The electrochemical measurements were performed on a CHI 660 E. The system consists of the sample (1 cm × 2 cm) as the working electrode, a Hg/HgO (reference electrode) and a platinum wire (counter electrode). All experiments were carried out in 1 M KOH.

1.7. Sample Activation Methods.

The 100 cyclic voltammetry (CV) scans (0.8−1.8V_{RHE}, 50mV s^{-1}) were carried out in 1 M KOH to ensure the complete activation of the sample (Fig. S1).

1.8. Quantitative Analysis of Products.

The reaction products were analyzed by high performance liquid chromatography (HPLC, Shimadzu) equipped with a Shim-pack GWS C-18 reversed-phase column (4.6 × 150 mm, 5 μm particle size). The chromatographic separation temperature was 35 °C, and UV detection wavelength was 265 nm. For analysis, 20 μL of mixed samples were collected from the reaction cell and diluted to 2 mL with deionized water. HMF conversion, FDCA yield, and FE were calculated using the following equations, where F stands for Faraday's constant.

$$\text{HMF conversion (\%)} = \frac{\text{mole of consumed HMF}}{\text{mole of initial HMF}} \times 100\%$$

$$\text{FDCA yield (\%)} = \frac{\text{mole of FDCA formed}}{\text{mole of initial HMF}} \times 100\%$$

$$\text{FE of FDCA (\%)} = \frac{\text{mole of FDCA formed}}{\text{total charge pass}/(6 \times \text{F})} \times 100\%$$

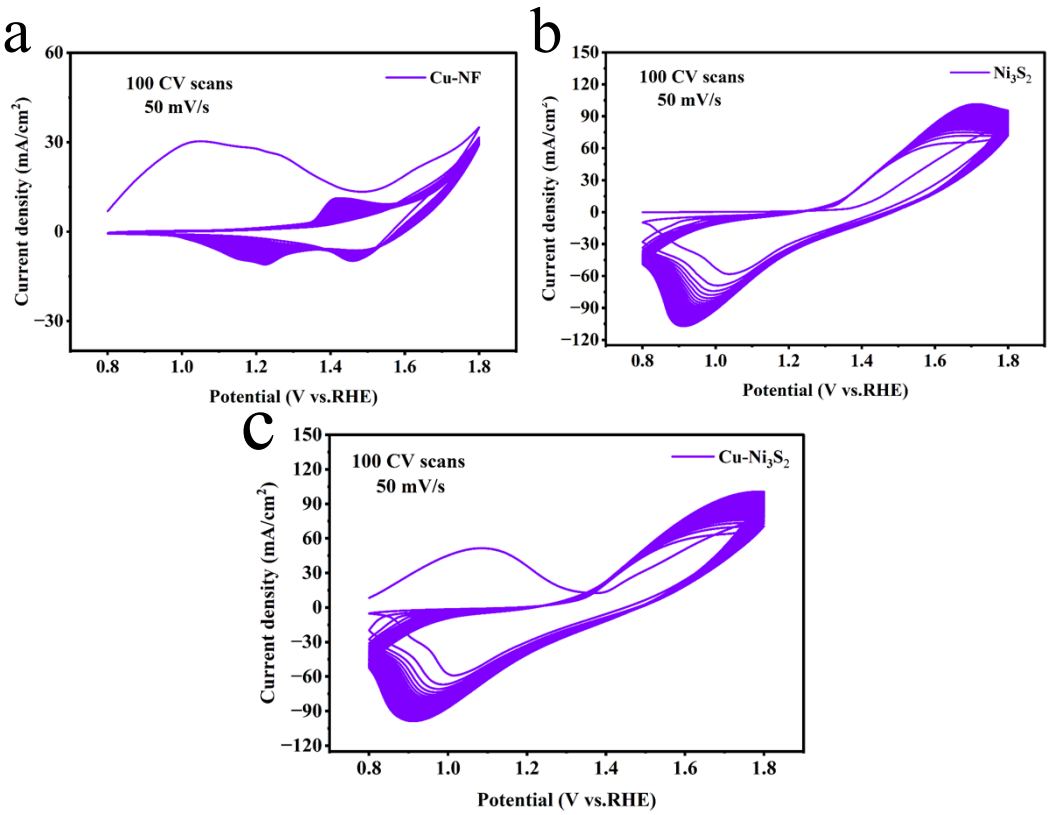

Fig. S1. CV curves of (a) Cu-NF, (b) Ni_3S_2, and (c) Cu-Ni_3S_2 at 50 mV/s in 1 M KOH.

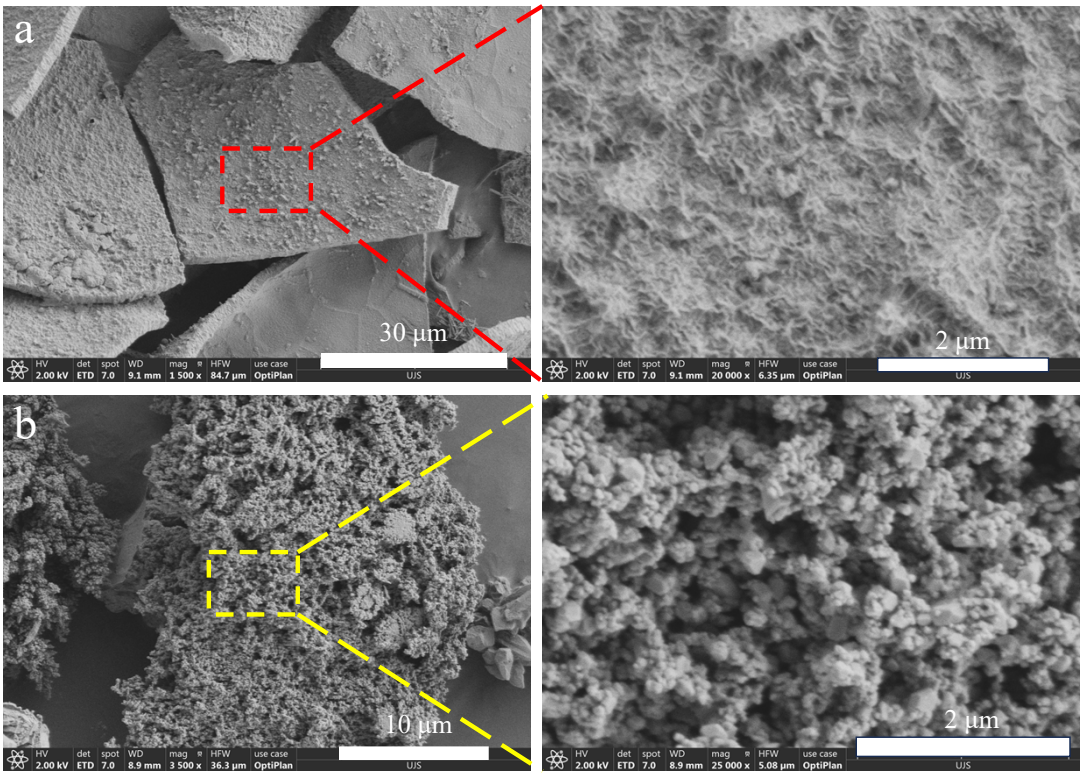

Fig. S2. SEM images of (a) Cu-NF, (b) Ni_3S_2.

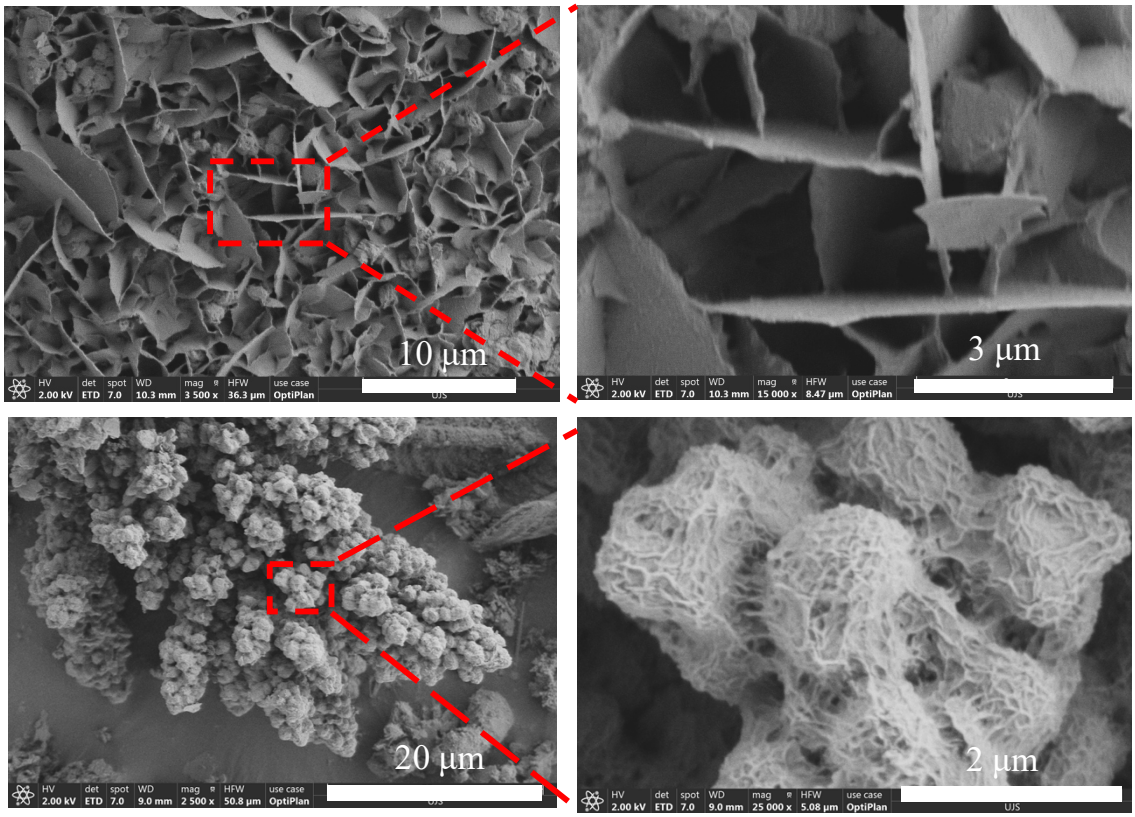

Fig. S3. SEM images of (a) Cu-Ni_3S_2, (b) activated Cu-Ni_3S_2.

a

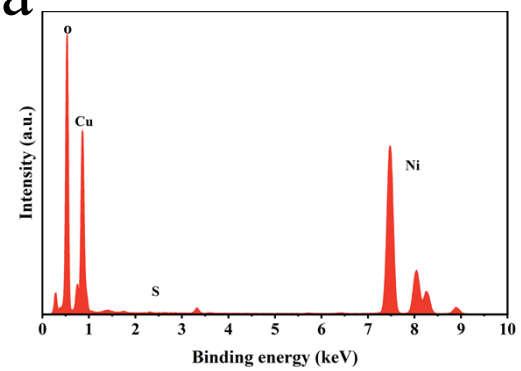

b

Element	Mass(%)	Atom (%)
O	28.19	59.4
S	0.11	0.12
Ni	55.5	31.88
Cu	16.2	8.6
Total	100	100

Fig. S4. Energy dispersive spectroscopy (EDS) of Cu-Ni_3S_2.

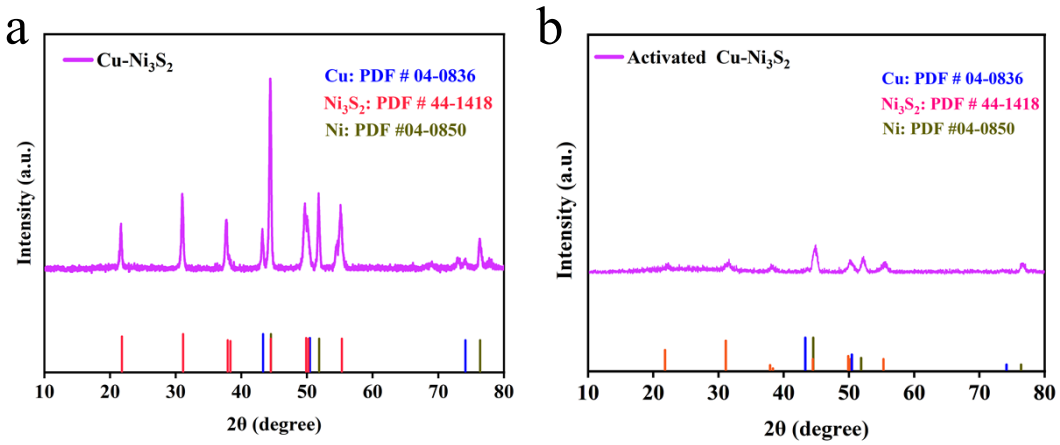

Fig. S5. XRD images of (a) Cu-Ni_3S_2, and (b) activated Cu-Ni_3S_2.

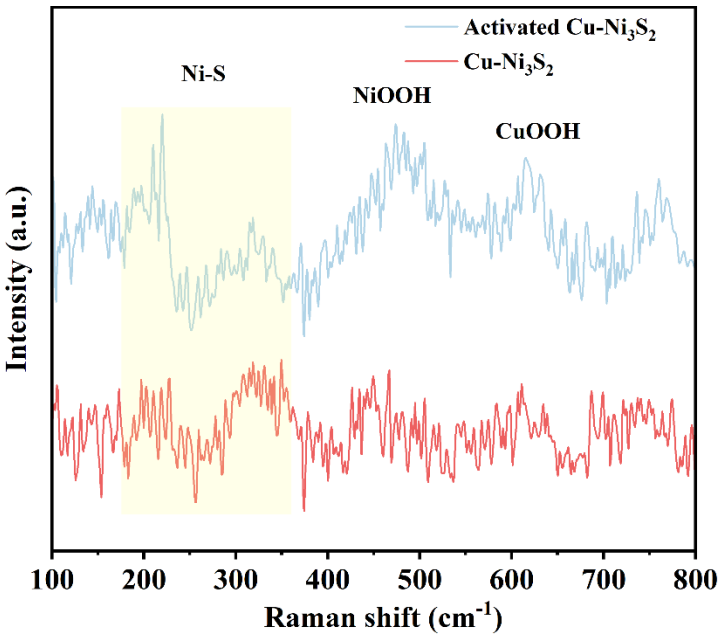

Fig. S6. Raman shift of $Cu\text{-}Ni_3S_2$ and activated $Cu\text{-}Ni_3S_2$.

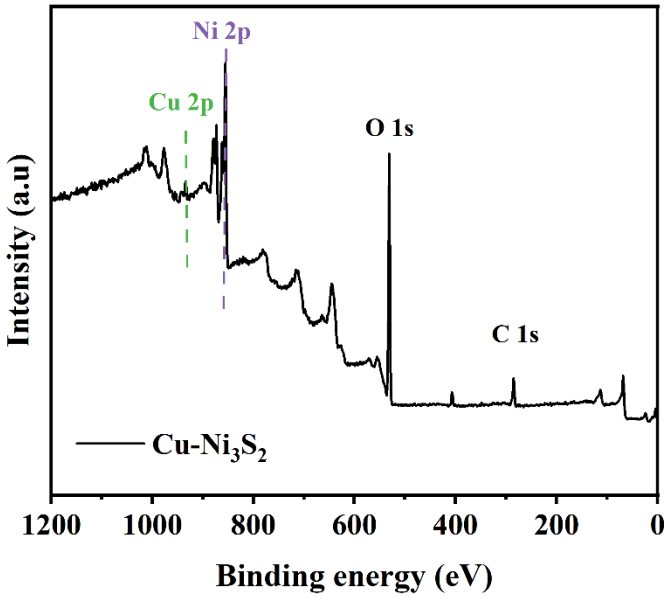

Fig. S7. Full-scan XPS spectra of Cu-Ni_3S_2.

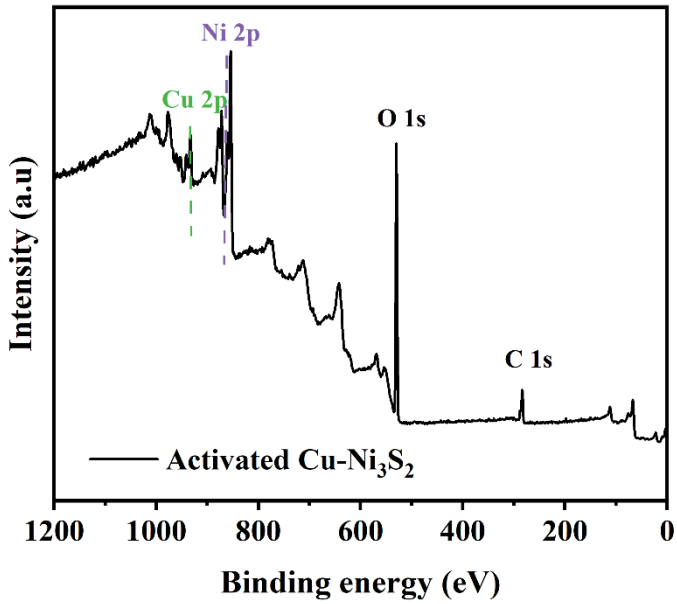

Fig. S8. Full-scan XPS spectra of activated Cu-Ni_3S_2.

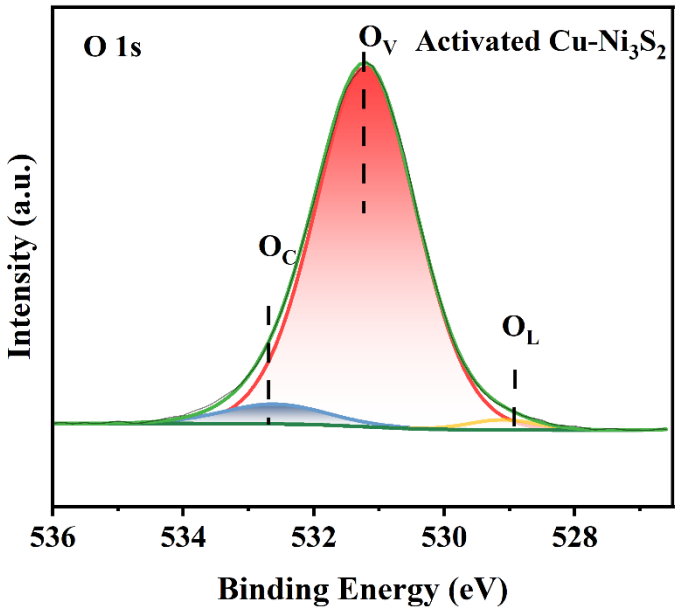

Fig. S9. XPS spectra of O 1s for activated Cu-Ni_3S_2.

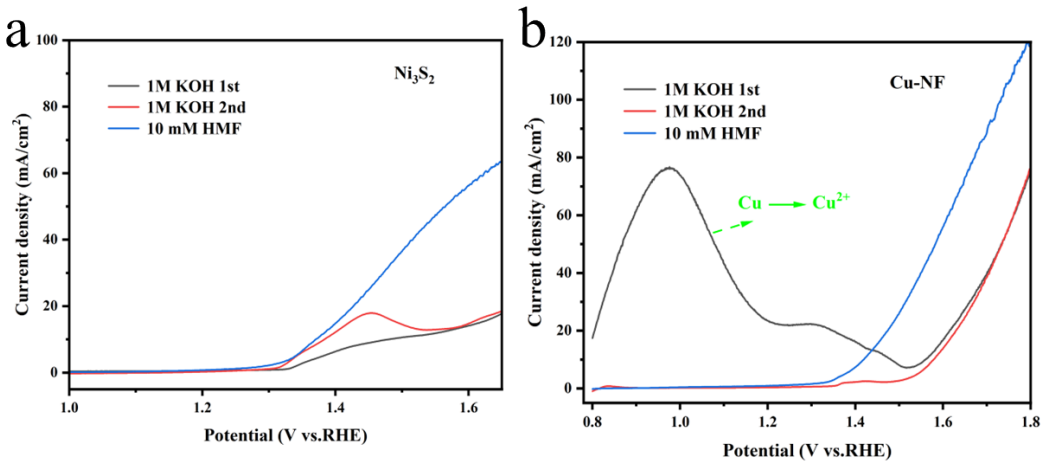

Fig. S10. LSV curves of (a) Ni_3S_2, and (b) Cu-NF with and without 10 mM HMF.

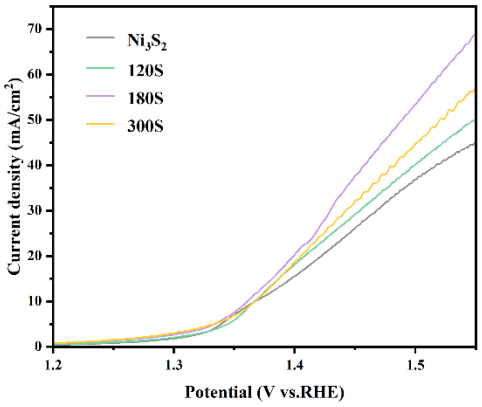

Fig. S11. LSV curves of Cu-Ni_3S_2 at different electrodeposition times for Cu.

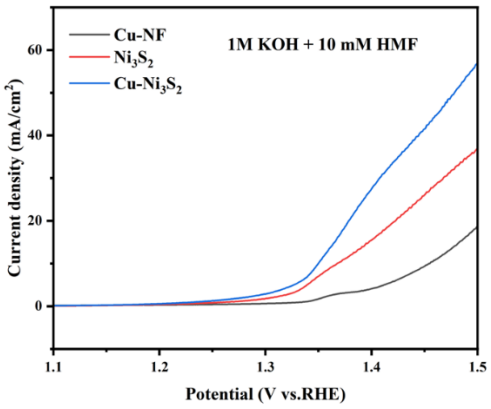

Fig. S12. LSV curves of Cu-NF, Ni_3S_2 and Cu-Ni_3S_2 in 1 M KOH and 10 mM HMF.

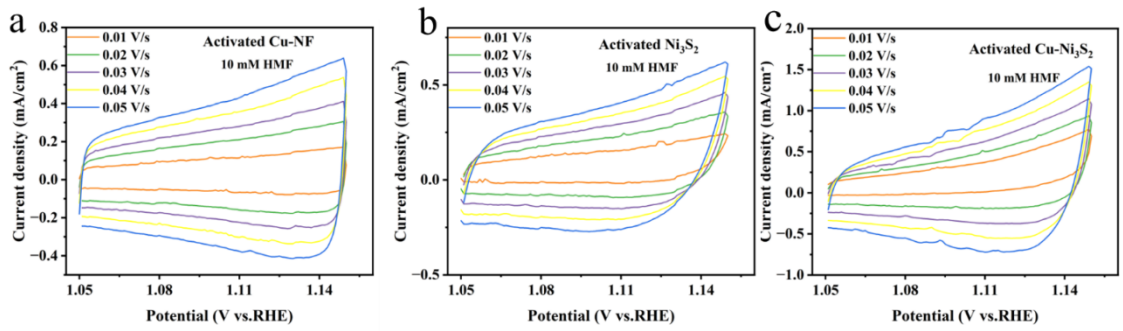

Fig. S13. CV curves of (a) activated Cu-NF (b) activated Ni_3S_2, and (c) activated Cu-Ni_3S_2 at different scan rates.

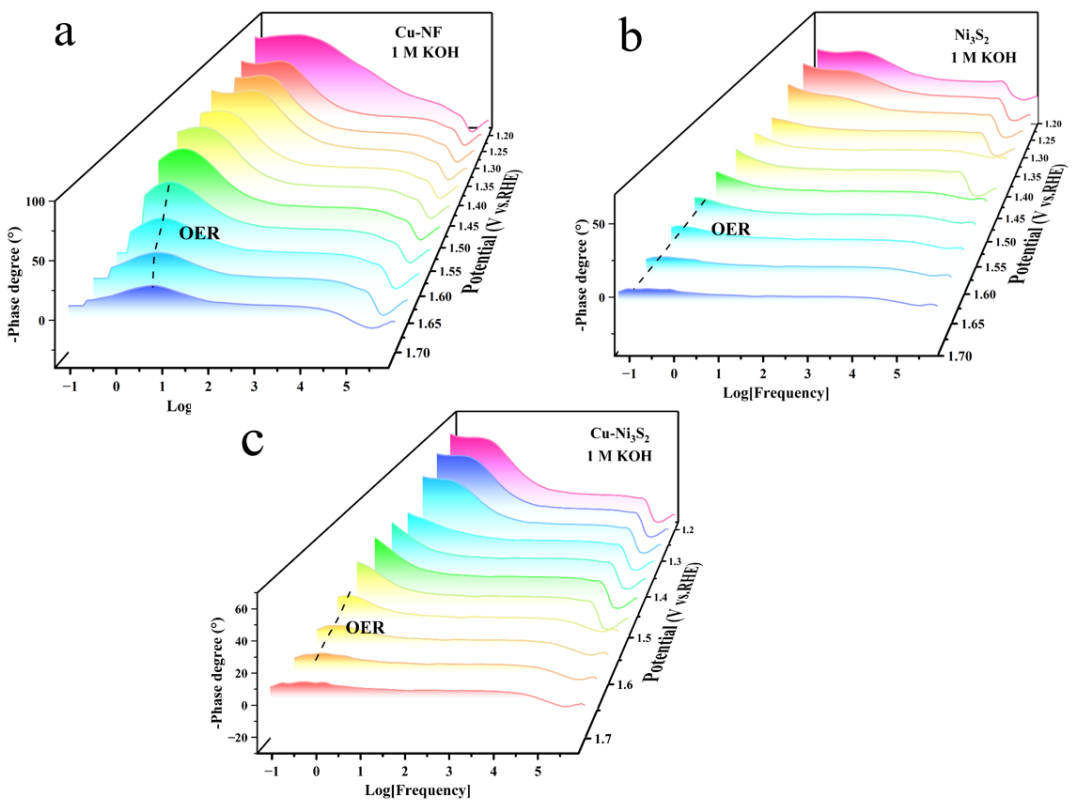

Fig. S14. Operando EIS spectra of (a) Cu-NF, (b) Ni_3S_2, and (c) Cu-Ni_3S_2 under different potentials in 1 M KOH.

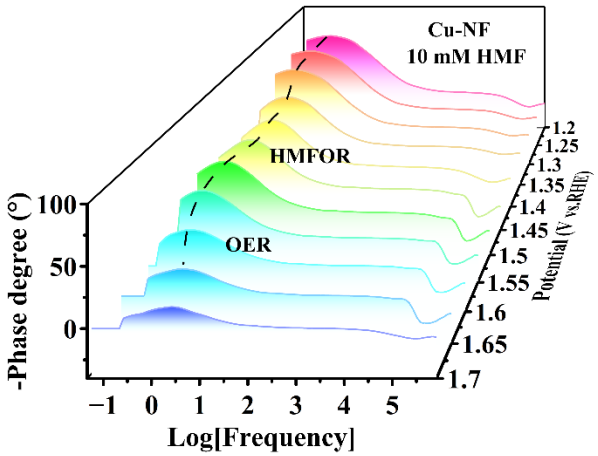

Fig. S15. Operando EIS spectra of Cu-NF under different potentials in 10 mM HMF.

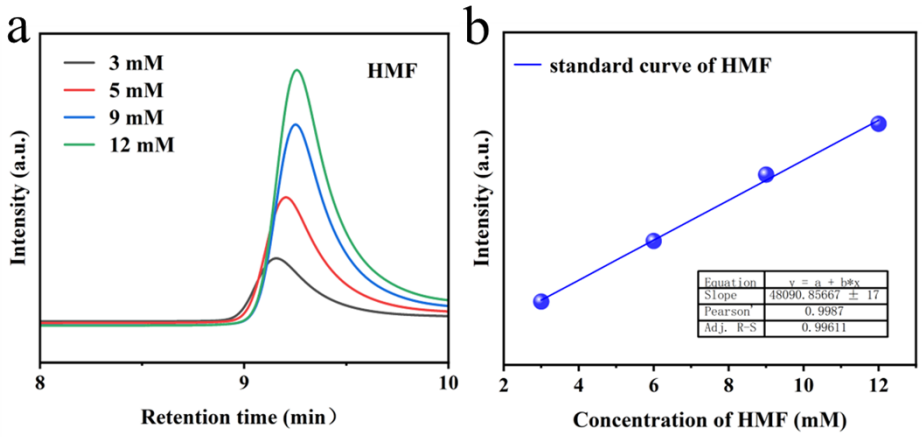

Fig. S16. (a) HPLC measurement, and (b) calibration curve of HMF.

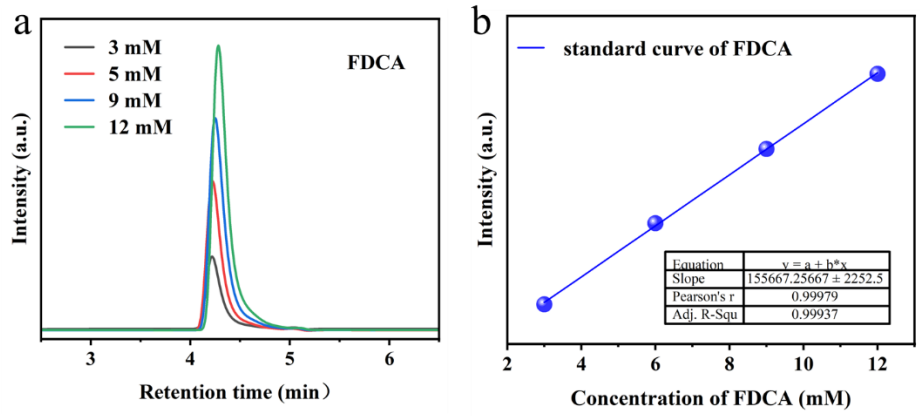

Fig. S17. (a) HPLC measurement, and (b) calibration curve of FDCA.

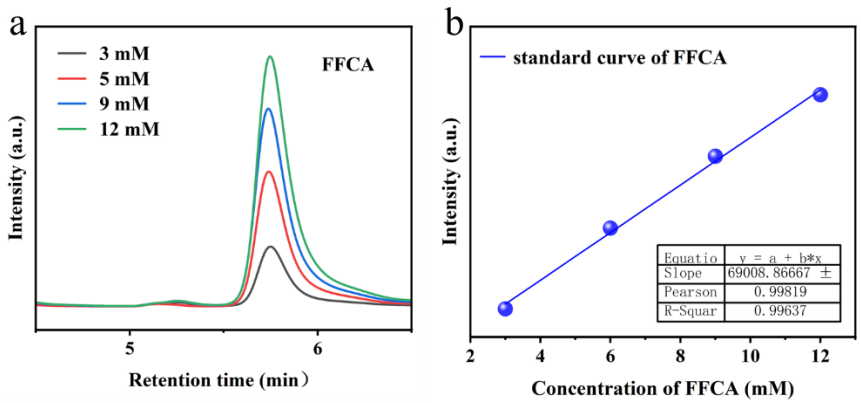

Fig. S18. (a) HPLC measurement, and (b) calibration curve of FFCA.

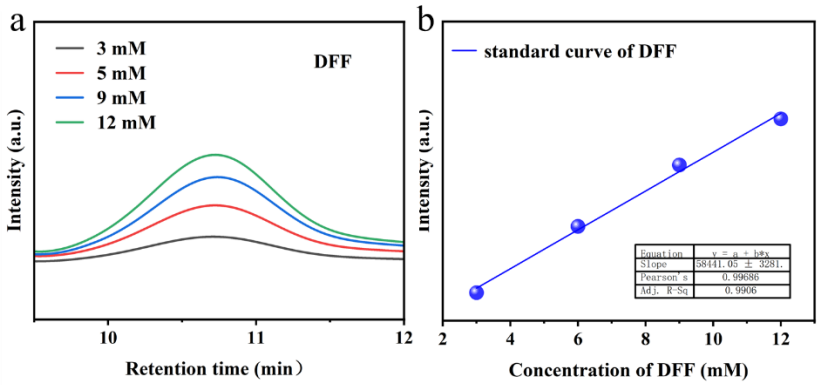

Fig. S19. (a) HPLC measurement, and (b) calibration curve of DFF.

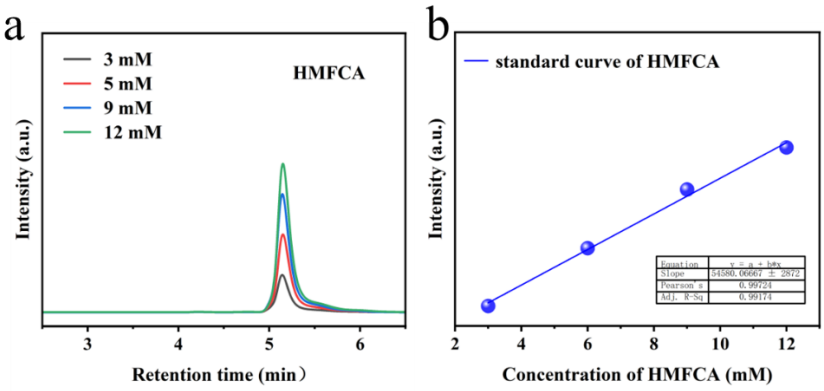

Fig. S20 (a) HPLC measurement, and (b) calibration curve of HMFCA.

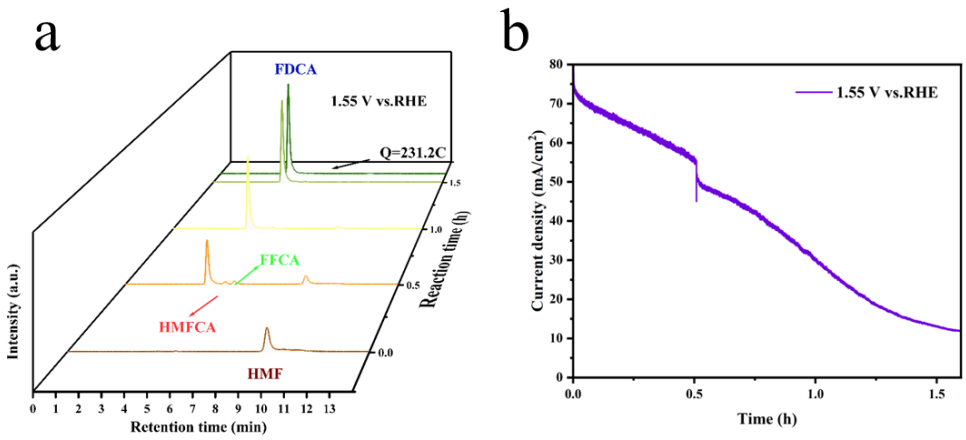

Fig. S21. (a) HPLC chromatograms (1.55 V_{RHE}, 10 mM HMF, 1 M KOH) of the activated Cu-Ni_3S_2. (b) The curve of current density vs time over the activated Cu-Ni_3S_2

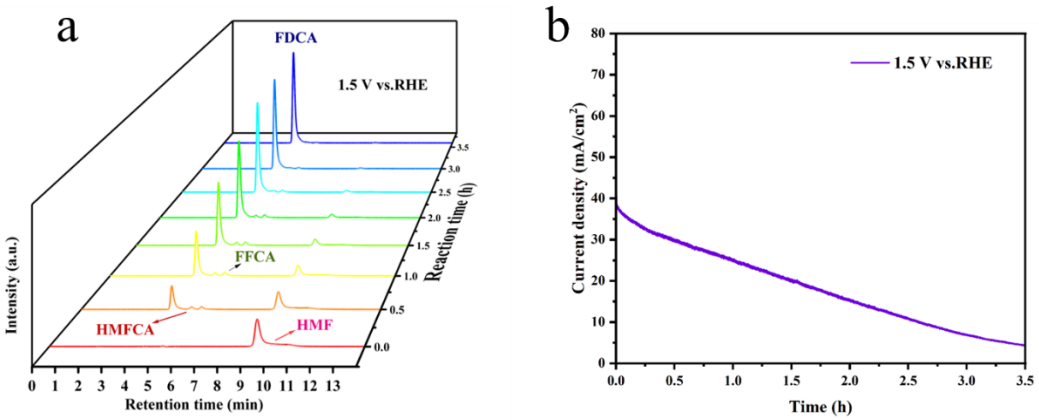

Fig. S22. (a) HPLC chromatograms (1.50 V_{RHE}, 10 mM HMF, 1 M KOH) of the activated Cu-Ni_3S_2. (b) The curve of current density vs time over the activated Cu-Ni_3S_2

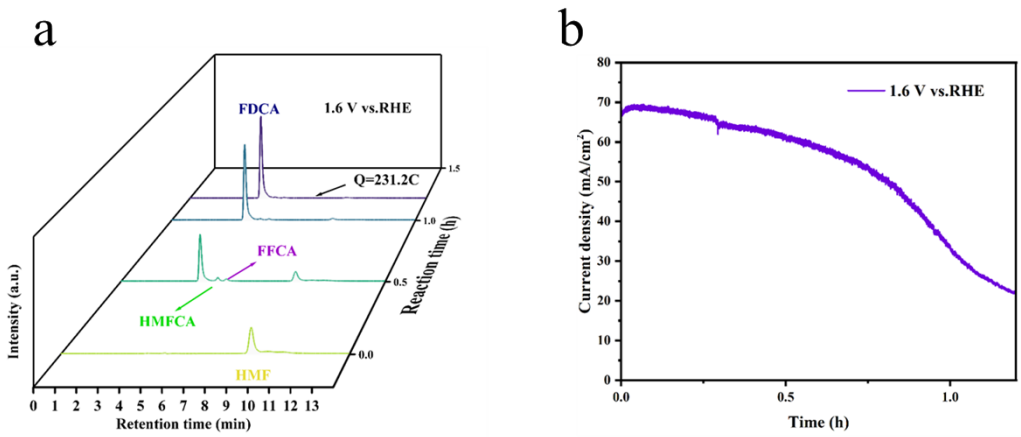

Fig. S23. (a) HPLC chromatograms (1.6 V_{RHE}, 10 mM HMF, 1 M KOH) of the activated Cu-Ni_3S_2. (b) The curve of current density vs time over the activated Cu-Ni_3S_2

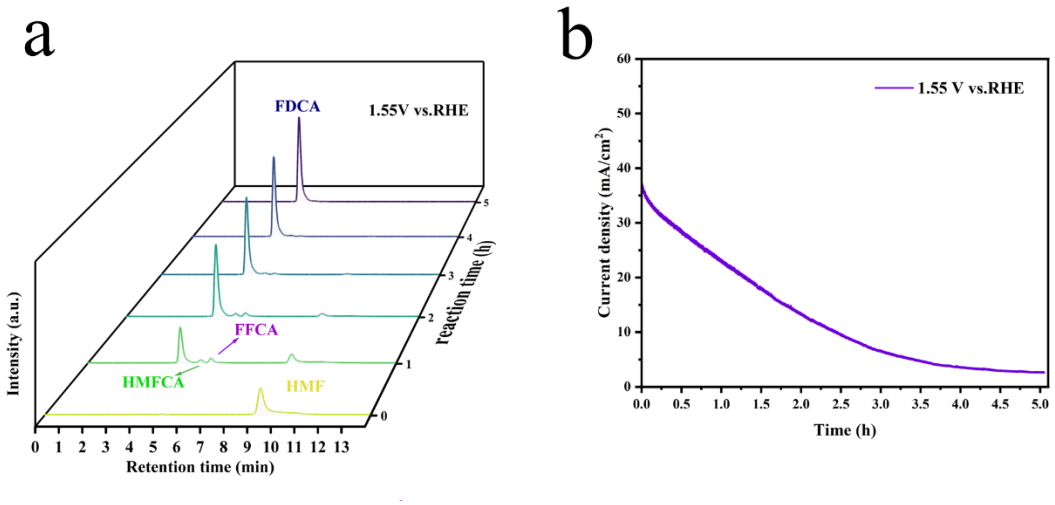

Fig. S24. (a) HPLC chromatograms (1.55 V_{RHE}, 10 mM HMF, 1 M KOH) of the activated Cu-NF. (b) The curve of current density vs time over the activated Cu-NF.

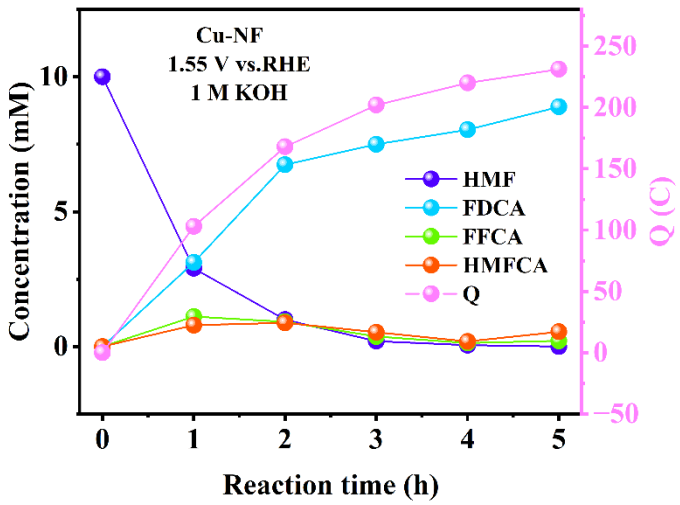

Fig. S25. Concentration of HMF, FDCA, HMFCA, FFCA, and total charge vs time over the activated Cu-NF at 1.55 V_{RHE} (1 M KOH, 10 mM HMF).

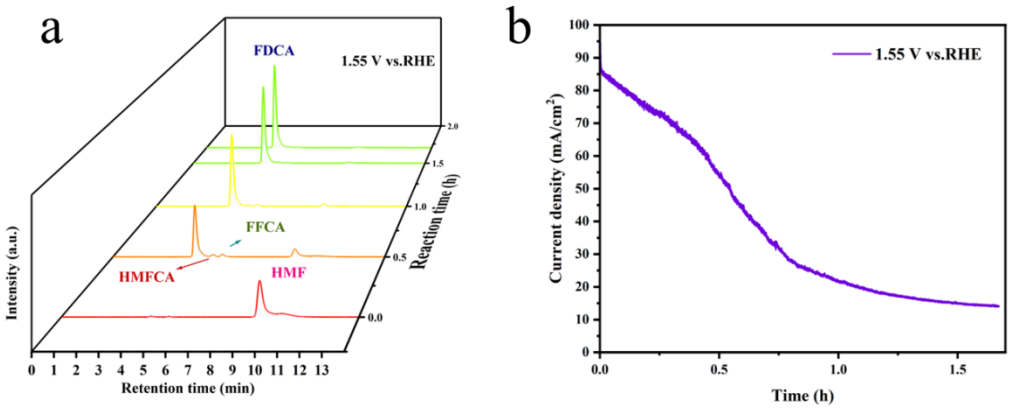

Fig. S26. (a) HPLC chromatograms (1.55 V_{RHE}, 10 mM HMF, 1 M KOH) of the activated Ni_3S_2. (b) The curve of current density vs time over the activated Ni_3S_2.

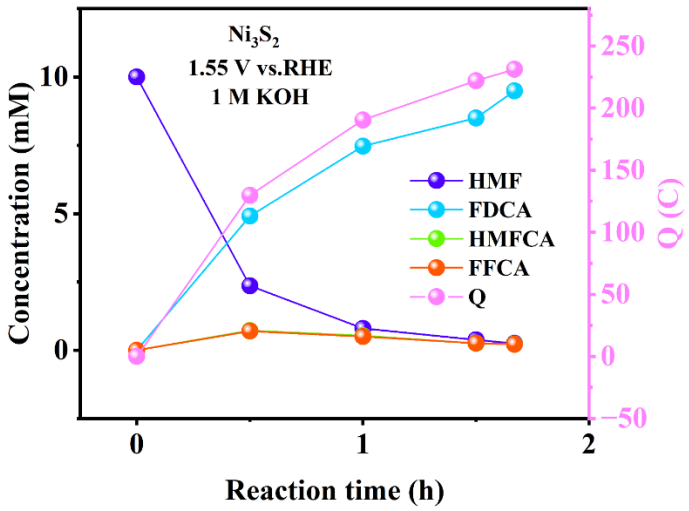

Fig. S27. Concentration of HMF, FDCA, HMFCA, FFCA, and total charge vs time over the activated Ni_3S_2 at 1.55 V_{RHE} (1 M KOH, 10 mM HMF).

Table S1. Results of Inductively Coupled Plasma (ICP) after Electrolysis

Total electrolyte volume (mL)	Electrolyte volume for ICP-MS (mL)	Test element	Sample Element Content C (mg/L)
40	2	Ni	0.089
40	2	Cu	3.07

Table S2. Reported electrochemical Oxidation of HMF to FDCA systems.

HMF	FDCA yield (%)	FE (%)	Potential (vs. RHE)	KOH	Catalysts	Ref.
10 mM	99.2	97.3	1.34 V	1 M	W_{20}-Ni_3S_2@NF	[1]
10 mM	97.6	97.6	1.38 V	1 M	H-0.3Co-Ni_3S_2	[2]
20 mM	100	100	1.4 V	1 M	Cu/Ni_3S_2-R	[3]
50 mM	98.8	97.6	1.45 V	1 M	Ni_3S_2/NF	[4]
10mM/L	98.1	98.8	1.42 V	1 M	P-Ni_3S_2/Ni/NF	[5]
100 mM	97.6	94.2	1.40 V	1 M	Mn0.2NiS/GF	[6]
20 mM	84	84	1.40 V	1 M	Ni_3S_2−Co_9S_8/CoLDH/NF	[7]
10 mM	98	100	1.45 V	1 M	NiS_X/CB-2	[8]
20 mM	98	98	1.5 V	1 M	Ni_3S_2/NiO_x	[9]
10 mM	99	99	1.45 V	1 M	$Co_{0.4}$NiS@NF	[10]
10 mM	100	100	1.45V	1 M	Co_9S_8-Ni_3S_2/Cu	[11]
10 mM	100	100	1.55 V	1 M	Cu-Ni_3S_2	**This work**

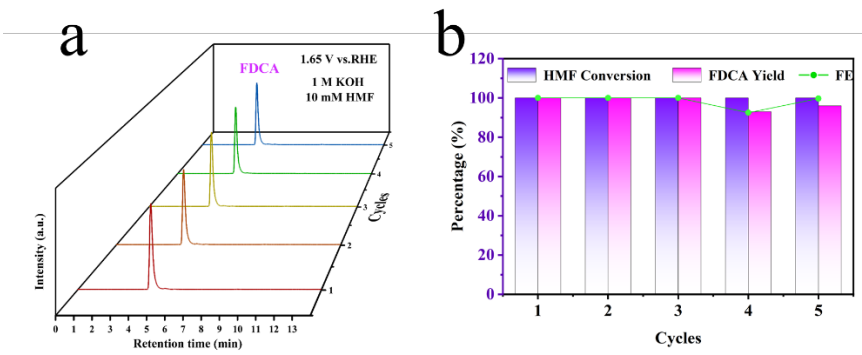

Fig. S28. (a) HPLC chromatograms of 5 cycles. (b) HMF conversion, FDCA yield and FE over activated Cu-Ni_3S_2 during 5 successive of HMF oxidation (1.55 V_{RHE}, 10 mM HMF, 1.0 M KOH).

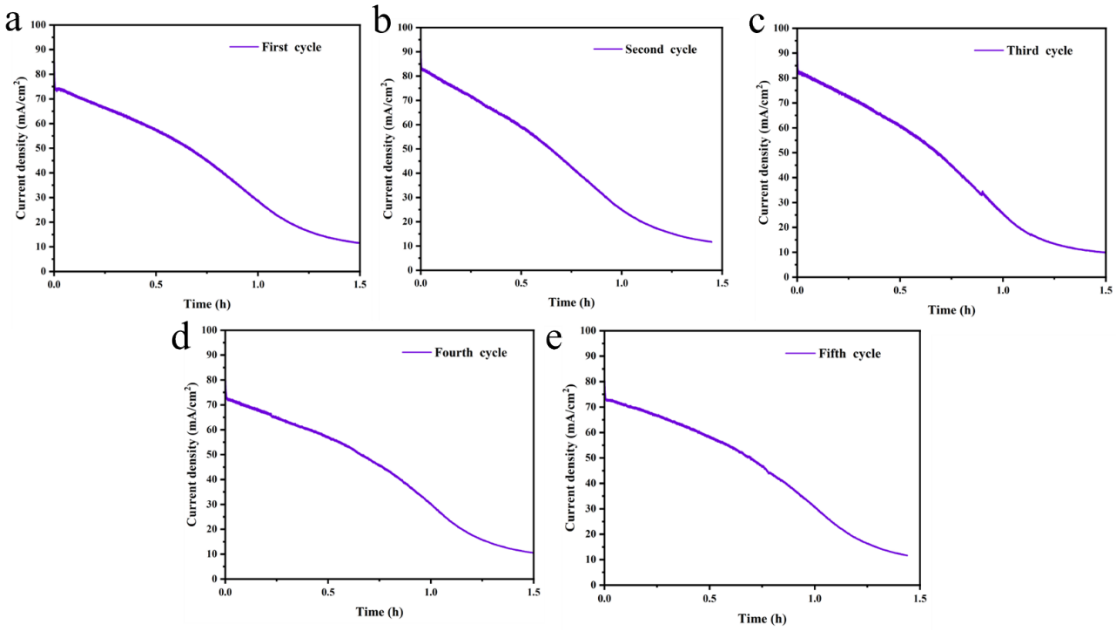

Fig. S29. The curve of current density vs time for 5 cycles.

References

1. S. Wang, G. Yang, Y. Jiao, Y. Liu, C. Tian, A. Wu, H. Yan, Tuning electronic structure of Ni_3S_2 with tungsten doping for high-performance electrooxidation of 5-hydroxymethylfurfural, *Sci. China Chem*., 2023, **66**, 3636-3644.
2. X. Zhang, Y. Li, J. Wang, G. Zeng, Q. Zhong, H_2O_2-assisted fabricate nickel cobalt sulfide as the efficient catalyst for the novel strategy of 5-hydroxymethylfurfural stepwise electrolysis, *Appl. Surf. Sci*., 2023, **639**, 158198.
3. P. Xu, Z. Bao, Y. Zhao, L. Zheng, Z. Lv, X. Shi, H. Wang, X. Fang, H. Zheng, Anionic Regulation and Heteroatom Doping of Ni-Based Electrocatalysts to Boost Biomass Valorization Coupled with Hydrogen Production, *Adv. Energy Mater*., 2024, **14**, 2303557.
4. L. Chen, Z. Yang, C. Yan, Y. Yin, Z. Xue, Y. Yao, S. Wang, F. Sun, T. Mu, Modulating Ni–S coordination in Ni_3S_2 to promote electrocatalytic oxidation of 5-hydroxymethylfurfural at ampere-level current density, *Chem. Sci.*, 2024, **30**, 12047-57.
5. M. Liu, J. Yin, C. Wang, W. Wang, Y. Gao, M. Yan, P. Geng, P doped Ni_3S_2 and Ni heterojunction bifunctional catalysts for electrocatalytic 5-hydroxymethylfurfural oxidation coupled hydrogen evolution reaction, *Chin. Chem. Lett.*, 2025, **36**, 111271.
6. S. Li, S. Wang, Y. Wang, J. He, K. Li, Y. Xu, M. Wang, S. Zhao, X. Li, X. Zhong, J. Wang, Doped Mn Enhanced NiS Electrooxidation Performance of HMF into FDCA at Industrial-Level Current Density, *Adv. Funct. Mater*., 2023, **24**, 2214488
7. T. Zhang, M. Xiang, X. Yang, C. Fu, Z. Yan, Z. Xu, Ni_3S_2–Co_9S_8 Heterojunction Integrated within Cobalt Layered Double Hydroxide Nanosheets for 5-Hydroxymethylfurfural Oxidation and Oxygen Evolution Reaction, *ACS Appl. Nano Mater*., **2025**, 8, 7278-89.
8. C. Yi, J. Li, Z. Liu, Ni_SX/carbon black hybrids for efficient electrochemical oxidation of 5-hydroxymethyfurfural to 2,5-furandicarboxylic acid, Catal. Today, 2025, 443, 114967.
9. Y. Zhang, J. Kuang, J. Yu, Y. Dong, J. Li, T. Xue, J. Wu, J.C Ma, J. Wan, S. Zeng, Y. Sun. Y. Zhang, J. Dong, L. Peng, S. Yang, J. Li, Construction of nickel and sulfur co-doped carbon nanotubes derived from hydrogen-bonded organic frameworks for

efficient biomass electrooxidation, *J. Mater. Chem. A*, 2024, **42**, 28853-62.

10. Y. Sun, J. Wang, Y. Qi, W. Li, C. Wang, Efficient Electrooxidation of 5-Hydroxymethylfurfural Using Co-Doped Ni_3S_2 Catalyst: Promising for H_2 Production under Industrial-Level Current Density, *Adv. Sci*., 2022, **9**, 2200957.
11. N. Wang, L. Wang, S. Yang, G. He, Y. Liu, H. Jin, Interface engineering of Co_9S_8-Ni_3S_2/Cu heterogeneous electrocatalyst for enhanced HMF oxidation, *Appl. Surf. Sci*., 2025, **689**, 162401.